# Chemical hydrogen insertion into γ-manganese dioxide exhibiting low microtwinning

**Lachlan A. H. MacLean and Frank L. Tye**

*Energy Technology Centre, Middlesex University, Bounds Green Road, London, UK N11 2NQ*

Hydrogen has been inserted by chemical methods into a synthetic $\gamma$-manganese dioxide characterized by 41% de Wolff disorder and a low amount of microtwinning. 23 Compounds covering the insertion range $0.00 \leqslant s \leqslant 0.82$ where $s$ is the value in $MnO_{1.966}H_s$ were prepared. Both XRD and FTIR evidence indicated homogeneous insertion in the range $0.00 \leqslant s \leqslant 0.34$ followed by heterogeneous reaction in the range $0.34 \leqslant s \leqslant 0.82$. Starting from the position that the structure of the predominant ramsdellite type lattice may be characterized by the distance $z$ between the apical oxygens normal to the $c$ axis of the manganese occupied octahedra and the angle $\beta$ that the apical vector makes with the $b$ axis a map was developed enabling the structure of the inserted compounds to be followed. In the homogeneous range, where $H^+$ and e are mobile, insertion led to expansion of $z$ with little change in $\beta$ whereas in the heterogeneous range, where $H^+$ is relatively immobile in the final product, a large change in $\beta$ was observed which is believed to result from the location of $H^+$ in the final product.

Chemical insertion of hydrogen into EMD (electrodeposited manganese dioxide), which is widely used as the cathode in primary alkaline manganese and Leclanché batteries, has been the subject of previous investigations.[1–4] These have generally focused on materials showing a large degree of structural disorder which are the most battery active forms of $\gamma$-manganese dioxide. Such materials are now understood to belong to a structural continuum *i.e.* $\gamma$-manganese dioxide. The continuum is characterized by varying proportions of two types of random structural disorder namely de Wolff disorder and microtwinning.[5] Commercial EMD typically has a microtwinning degree of *ca.* 100% and *ca.* 40% de Wolff disorder. Hydrogen insertion initially leads to the formation of a near ideal solid solution with $H^+$ and e present as mobile thermodynamically independent entities.[6] Beyond a certain level of insertion, evidence for clustering of $H^+$ and e pairs has been accumulated with the ineluctable formation of stable microdomains of the end product containing located and relatively immobile $H^+$ as detected by FTIR spectroscopy.[7] It has been proposed that the formation of such regions causes anisotropic expansion of the structure and an accompanying demicrotwinning of the structure as evidenced by the appearance of new lines in the XRD pattern.[8]

Less attention has been given to other possible members of the structural continuum particularly regarding chemical insertion of H with the notable exception of the work by Giovanoli and co-workers.[4] In the present work a material possessing a low microtwinning fraction (*ca.* 17%) and *ca.* 40% de Wolff disorder produced by the suspension bath process[9] has been investigated. The principal difference between materials containing low microtwinning percentages and those with high microtwinning percentages is in the number of peaks observable in their XRD patterns. Essentially, highly microtwinned materials contain peaks which are combinations of broadened and shifted lines whereas these lines are distinct in their low microtwinned counterparts. In consequence a typical EMD has only six broad peaks in the $2\theta$ range 15–70° (Cu-K$\alpha$) whereas low microtwinned materials contain at least twice this number many of which are inherently sharper. Thus changes in XRD patterns which occur with H-insertion yield in principle more information with low microtwinned materials and this information may in turn advance understanding of the highly microtwinned counterparts. A feature of this examination was the large number of samples at differing insertion levels compared to previous work.

## Experimental

### Material characterisation

The low microtwinned $\gamma$-manganese dioxide material investigated in this work was an EMD produced by the suspension bath process[9] (SBPA). It is characterized by the physicochemical properties given in Table 1.

### H-insertion

The insertion of H into $\gamma$-manganese dioxide may be represented as:

$$MnO_n + sH^+ + se \rightarrow MnO_nH_s \quad (1)$$

where $n$ reflects the non-stoichiometry of the starting compound and $s$ the level of H insertion. For material SBPA, $n = 1.966$, which implies that $s$ may range from zero to $s = 0.932$ for full H-insertion. Two chemical methods were used to insert H. The first involved contact with acetone at room temperature and was used to produce compounds with a small amount of H-insertion (*i.e.* from $s = 0.000$ to $s = 0.120$). Acetone, which had previously been thought to be inert as it was used to wash samples of manganese dioxide in preparation for TEM studies,[10] has been found to be a suitable reductant[2] for $MnO_2$. It reacted quickly with SBPA (*i.e.* reaction times of minutes were used to produce the above mentioned samples) but was unable to produce high levels of H-insertion even under reflux. For higher levels of H-insertion reflux in propan-1-ol, as described elsewhere, was used.[7] Fig. 1 indicates the rate of reaction of SBPA under reflux where an approximate fivefold excess of propan-1-ol was used, based on the reaction:

$$MnO_2 + CH_3CH_2CH_2OH \rightarrow MnOOH + CH_3CH_2CH_2O \quad (2)$$

**Table 1** Physicochemical and structural properties of SBPA

| property | | ref. |
|---|---|---|
| $n$ in $MnO_n$ | 1.966 | 8 |
| % microtwinning | 17 | 8 |
| % de Wolff disorder | 41 | 8 |
| BET surface area/$m^2\ g^{-1}$ | 22[a] | 9 |

[a]Obtained from Fig. 8 in ref. 9 which displays the relationship between BET surface area and geometrical current density of deposition for SBP-EMD, which for material SBPA = 1.2 A $dm^{-2}$.

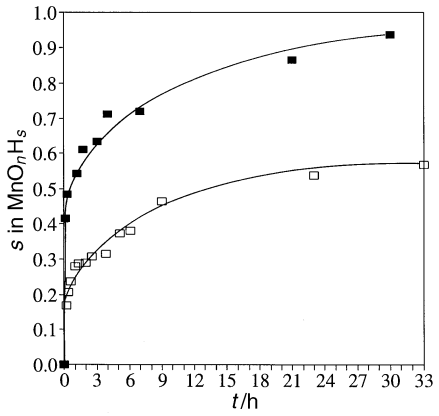


**Fig. 1** Comparison of the rate of reactions of SBPA (□) and IBA 19 (■) in boiling propan-1-ol

After 33 h of reflux the insertion is only 41% complete. This may be compared to a typical commercial EMD (*i.e.* one with *ca.* 100% microtwinning), International Battery Association common sample 19 which is completely filled after 24 h of reflux, see Fig. 1. Approximately six weeks of reflux were required to produce a compound approaching full insertion. Such long reaction times tended to form small quantities of $Mn_3O_4$ or possibly $\gamma$-$Mn_2O_3$ (which has a similar XRD profile) which was believed to result from a side-reaction. A higher boiling alcohol (butan-1-ol) was therefore used to produce deeply inserted compounds. The highest insertion level achieved free from $Mn_3O_4$ was $s=0.814$, 87% of the maximum theoretical limit. The total number of samples produced covering the insertion range $0.00 \leqslant s \leqslant 0.82$ was 23.

### Chemical analysis

The level of H-insertion was determined by the double titration method of Vetter and Yeager[11] which enables both the available oxygen and total manganese to be determined on a single sample. Each level of H-insertion was the average of two determinations.

### XRD

XRD patterns were obtained with a Philips PW 1700 powder X-ray diffractometer system which was used optimally configured for the collection of generally weak $\gamma$-manganese dioxide patterns. A Cu target broad focus tube (PW 2253/20) with 1° scatter and divergence slits and a 0.1 mm receiving slit was employed. Scans were recorded at a $2\theta$ scan rate of $0.01^\circ\ s^{-1}$. Samples were ground for 3 min by hand in an agate mortar and pestle and mounted by a backfilling procedure in flat aluminium holders. Peak positions, which are the average of two measures, were determined using the Philips software package APD (automatic powder diffraction). The XRD traces presented use a smoothing factor of two as defined in APD.

### FTIR

Samples for FTIR spectroscopy were prepared by the following procedure. About 3 mg of each sample was mixed with about 450 mg of CsI. Approximately 200 mg of this mixture was used to produce compressed pellets of known mass. The spectrum were recorded on a Perkin Elmer PE 1750 FTIR spectrometer to give data of nominal resolution $4\ cm^{-1}$. A reference spectrum of CsI was subtracted and the spectra were normalised to $1\ mg\ cm^{-2}$ using the recorded masses.

## Results and Discussion

### Evidence from XRD for homogeneous and heterogeneous regions of H-insertion

The XRD results provide a clear unambiguous interpretation of the nature of H-insertion. Initially a solid solution is formed over a restricted range of insertion and thereafter H-insertion occurs by a heterogeneous solid state reaction. Fig. 2 presents a selection 17 of the 23 XRD patterns covering the full insertion range. The structure of the final compound is intimately related to the structure of the starting material[8] and contains essentially the same number of lines (with the same indices) in different positions due primarily to expansion in the *b* orthorhombic direction as indicated in Fig. 3. Both starting and fully H-inserted structures are of the diaspore type with selective broadening of lines with $\frac{1}{2}k+l$ odd due to de Wolff disorder.[12] The structure of the fully H-inserted compound has been denoted $\delta$-MnOOH.[3,8]

The principal XRD evidence for the formation of a solid solution in previous works comes from the continuous shift in line position with insertion level. If a heterogeneous reaction was to occur after a given insertion level the expected variation in line position would lead to a shift in position followed by a region where the position was independent of insertion level. Fig. 4 shows the *d*-spacing of lines (021) and (121) *versus* insertion level and confirms that the above description holds, the heterogeneous reaction beginning at $s=0.34$. The peaks were chosen such that they are sharp and expected to have a large shift with H-insertion (*i.e.* they cut the *b* axis at a steep angle) so that if a heterogeneous reaction resulted the peaks characterized by the end members of the process were well separated in *d*-spacing to avoid apparent peak movements due to closely overlapping peaks.

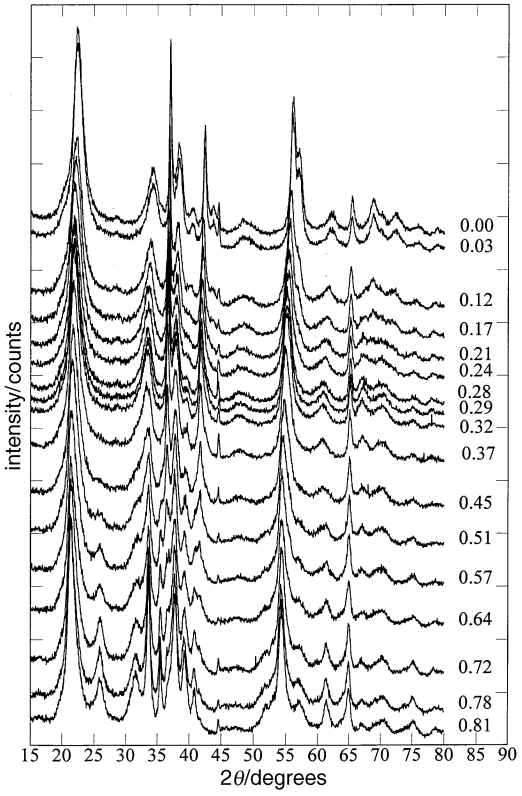


**Fig. 2** XRD patterns of the H-inserted materials stepped in proportion to their insertion level for material SBPA

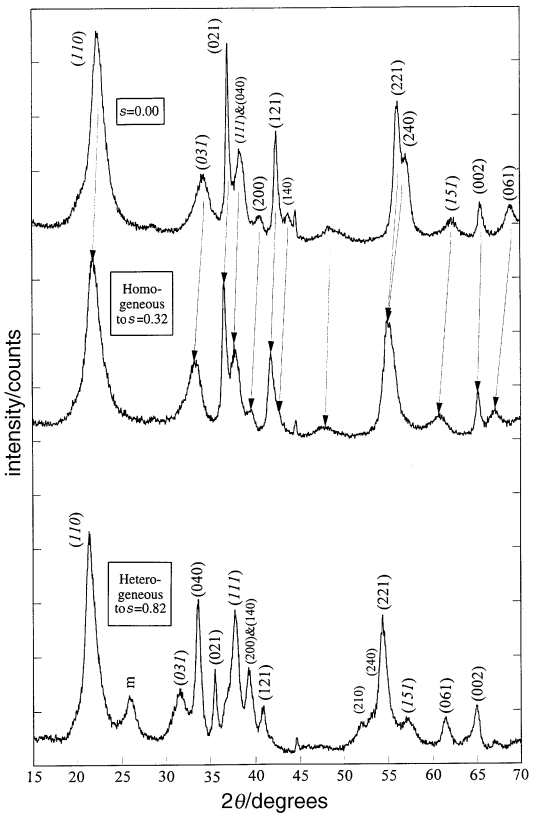


**Fig. 3** XRD patterns bounding the changes in the H-insertion reaction to material SBPA. Arrows indicate peak shifts in the homogeneous region. hkl, predominant orthorhombic lattice (sharp lines); *hkl*, broad lines; m, manganite impurity.

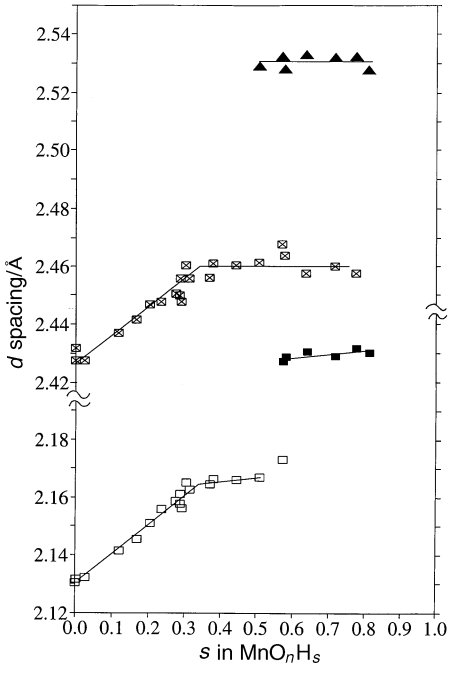


**Fig. 4** Interplanar spacing variation of peaks (021) and (121) with H-insertion level. R, derived from ramsdellite index, G, derived from groutite index. ☒, $(021)_R$; ▲, $(021)_G$; □, $(121)_R$; ■, $(121)_G$.

Further evidence from the XRD data for a heterogeneous reaction beyond a given insertion level comes from a comparison of the end members of this process. Fig. 5 compares the XRD patterns of the product and reactant of the heterogeneous insertion reaction as decided from the evidence of the *d*-spacing

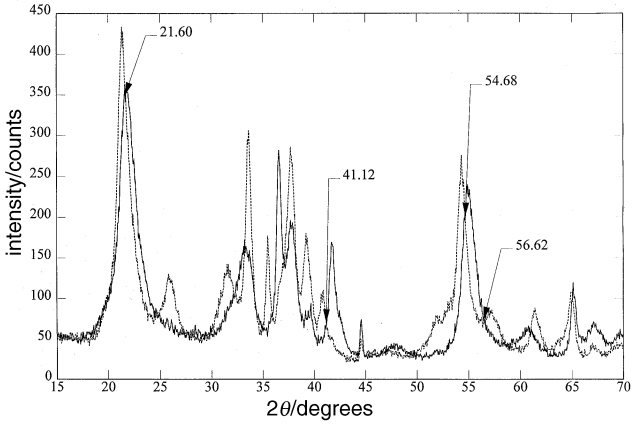


**Fig. 5** Comparison of the product and reactant XRD patterns for the heterogeneous H-insertion reaction with the positions of four isobestic points indicated

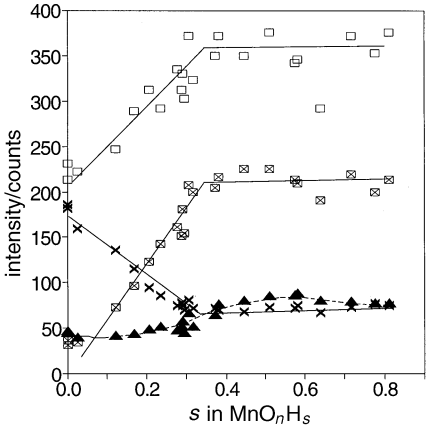


**Fig. 6** Intensity *vs.* insertion level at the $2\theta$ positions indicated in Fig. 5. □, 21.60° $2\theta$; ☒, 54.68° $2\theta$; ▲, 41.12° $2\theta$; ×, 56.62° $2\theta$.

variation described above. Clear isobestic points† are expected, four of which are indicated in the figure. Fig. 6 indicates the measured counts against insertion level at each of the four values of $2\theta$ indicated in Fig. 5. As expected the intensity at these values of $2\theta$ is virtually independent of insertion level in the heterogeneous region in contrast to the progressive change found in the homogeneous region.

Fig. 3 summarizes the effects on the XRD patterns of H-insertion into material SBPA.

## Evidence from FTIR for homogeneous and heterogeneous regions of H-insertion

Fig. 7 displays a selection of FTIR spectra in the range 400–4000 $cm^{-1}$ with increasing levels of H-insertion. Following previous work[7] the spectra are conveniently considered as two distinct parts, namely, the regions above and below 800 $cm^{-1}$. Below 800 $cm^{-1}$ the vibrations are believed to be due to the $[MnO_6]$ octahedra whereas above 800 $cm^{-1}$ they are concerned with various hydrous component vibrations. For heavily microtwinned EMD the spectra in the region $>800$ $cm^{-1}$ showed OH bond formation only above a given level of H-insertion.[7]

The interpretation of the FTIR data was facilitated by noting that the absorbance *versus* insertion level was nearly independent of insertion level at 488 $cm^{-1}$ and only slightly

† Isobestic points are points of intensity that are independent of composition. They normally occur at the crossover point of two overlapping peaks of a two-component system where one component transforms into the other.

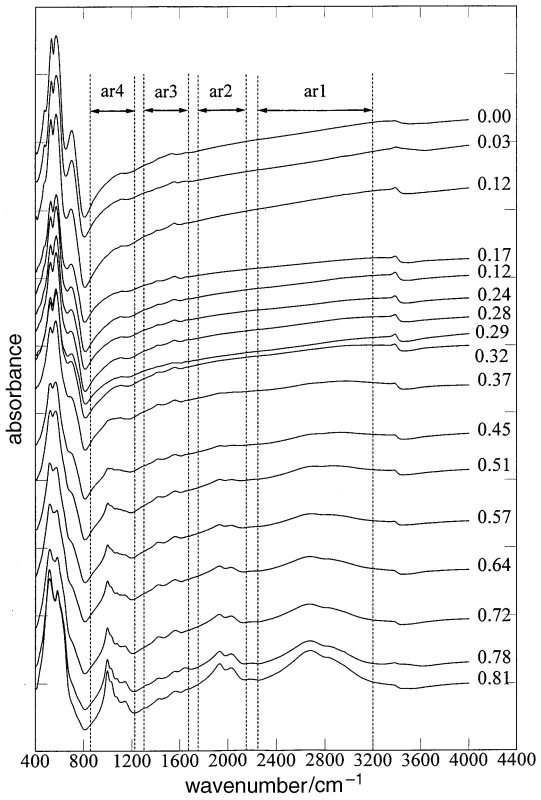


**Fig. 7** FTIR spectra of H-inserted SBPA materials stepped downwards in proportion to their insertion level

less so at 652 cm$^{-1}$. This suggested a normalisation procedure was valid. Each spectrum was therefore normalized across the whole wavenumber range so as to produce a constant value at 488 cm$^{-1}$ by the following procedure:

$$\text{Normalized abs.}(x)=\frac{0.682\ \text{abs.}(x)}{\text{abs.}(488)} \qquad (3)$$

where 0.682 is the average absorbance at 488 cm$^{-1}$ over all insertion levels.

In the case of the XRD intensity data, homogeneous followed by heterogeneous regions of H-insertion resulted in the intensity at isobestic values of $2\theta$ varying in the homogeneous region but becoming independent of insertion level in the heterogeneous part. For FTIR absorbance data however, variation in the homogeneous region is expected only if the environment of the vibrating system is continuously changing. Examination of the spectra reveals four wavenumbers where the absorbance is independent of insertion level beyond a given insertion level as shown in Fig. 8. In the case of the wavenumber at 600 cm$^{-1}$ a clear break is observed at $s=0.34$. The change in absorbance in the region $0.00\leqslant s\leqslant 0.34$ suggests that [$MnO_6$] octahedra are distorting with H-insertion. The absorbances at 964 and 1040 cm$^{-1}$ show less pronounced changes at the same H-insertion level. The absorbance at 652 cm$^{-1}$ shows no such break which accords with the unnormalized data which also was independent of insertion level across the whole insertion range as already mentioned. Not shown is the absorbance at 488 cm$^{-1}$ which is arranged to be independent of insertion level. The above findings indicate that a homogeneous reaction occurs for $0.00\leqslant s\leqslant 0.34$ and a heterogeneous reaction for $s\geqslant 0.34$ in agreement with the XRD evidence.

Fig. 9 shows the behaviour of the FTIR patterns in the heterogeneous region. Clear isobestic points are formed (at 600 and 652 cm$^{-1}$) from overlapping spectra whereas the spectra in the homogeneous region (see Fig. 7) indicate a

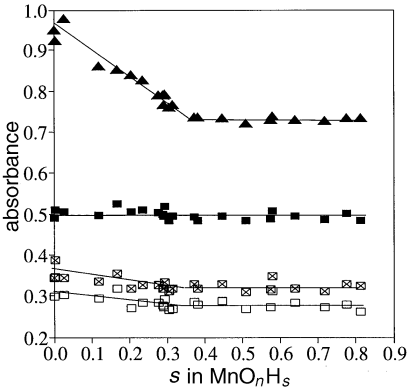


**Fig. 8** Absorbance *vs.* insertion level at four wavenumbers which are isobestic points beyond $s=0.34$. ▲, 600; ■, 652; □, 964; ⊠, 1040 cm$^{-1}$.

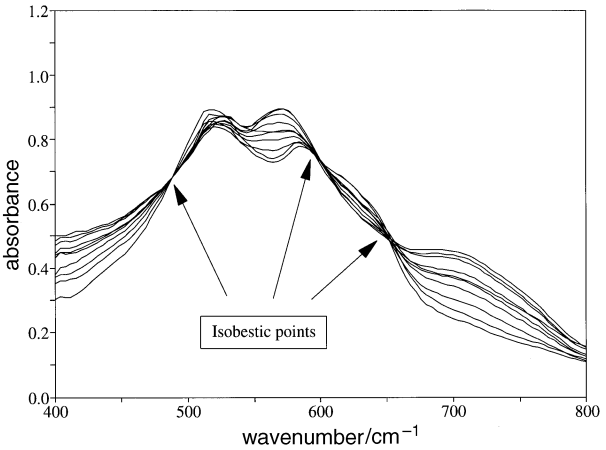


**Fig. 9** Normalized FTIR spectra (800–4000 cm$^{-1}$) of H-inserted SBPA for $0.34\leqslant s\leqslant 82$. Isobestic indicate that the H-insertion reaction was heterogeneous.

progressive shift in intensity (and peak position). Therefore the original crossover point used in the normalization procedure should not be regarded as an isobestic point but rather as a point of constant intensity arising from a fortuitous combination of peak shifting and intensity loss during homogeneous H-insertion.

## H-location in SBPA

Following Fitzpatrick *et al.*[7] FTIR spectra can provide evidence as to whether H is freely mobile or located in the crystal structure by measurement of peak areas minus background in the wavenumber regions giving rise to OH bond formation. Such measurements on H-inserted EMD compounds suggested that H is mobile in the structure up to $s=0.63$ (material coded R2) and $s=0.55$ (IBA 19) and thereafter located as a result of OH bond formation as evidenced by a steady increase in peak areas. The dotted lines shown on Fig. 7 indicate the positions of the boundaries used to measure the net integrated areas defined as area(1)−area(4) as used previously.[7] Fig. 10 indicates the result of this procedure for areas(1), (2) and (4). Area(3) is not shown as it was independent of insertion level and as in the case of heavily microtwinned EMD, the peaks in this region appear to be third-order overtones of the fundamental [$MnO_6$] octahedral vibrations.[7] Areas(1), (2) and (4), however, indicate an initial behaviour which is nearly independent of insertion level followed by a sharp change and increase with insertion level (Fig. 10). The change occurs at $s=0.34$ in accordance with the onset of heterogeneous reaction as presented above. This indicates that the final product of the

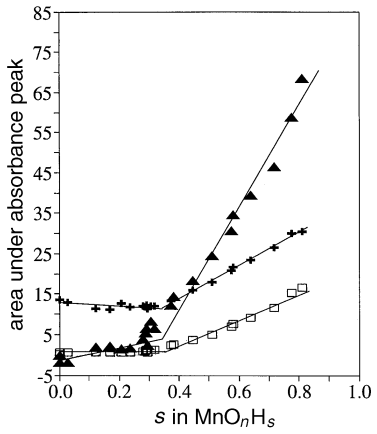


**Fig. 10** Integrated net peak areas as defined in Fig. 7 *vs.* H-insertion level. ▲, area 1; □, area 2; +, area 4.

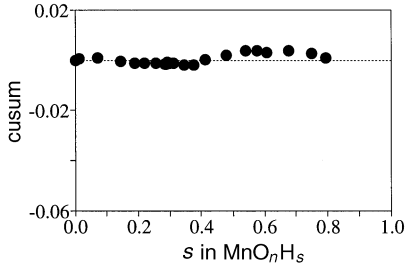


**Fig. 11** Modified cusum of absorbance *vs.* H-insertion level at 3800 cm$^{-1}$

heterogeneous reaction in the insertion region $0.34 \leqslant s \leqslant 0.82$ contains located H in contrast to the initial region $0.00 \leqslant s \leqslant 0.34$ which contains mobile H in a solid solution.

### De-microtwinning

For highly microtwinned materials (*ca.* 100%) it has been proposed that a de-microtwinning of the structure takes place at high H-insertion levels.[8] As a result a change in the rate of decrease of the background absorbance level occurred.[7] A modified cusum‡ procedure was used to detect and emphasize any change in slope. In contrast to highly microtwinned EMD, applying the same procedure to SBPA produced no large change in slope at a wavenumber unaffected by the growth of peaks connected with OH bond formation as presented in Fig. 11. The best straight line through the original absorbance *vs. s* data was chosen in the cusum procedure and the results are presented on a similar *y*-scale to that used previously where de-microtwinning was found.[8] Thus as expected no evidence of de-microtwinning is observed since the initial material has only low microtwinning (Table 1).

### Lattice parameter variation

The predominant orthorhombic lattice of the ramsdellite/groutite component of the intergrowth structure may be determined from the interplanar spacings of the 'sharp lines' ($\frac{1}{2}k+l$, even) which are unaffected by de Wolff disorder (see Fig. 3). It is necessary to choose a restricted subset of these lines ($S_{res}$), namely (021), (121), (221) and (002). This is because certain peaks rapidly become weak or merge into neighbouring peaks with insertion, see for example peaks (221) and (240) in Fig. 3. Even for a low microtwinned sample (as in this case) the values obtained by such a procedure depend on the choice of lines

‡ Cusum (cumulative sum) plots[13] are normally used in statistical quality control procedures to detect the changes in a quantity defined by an average to a new average as a result of some change to the system.

**Table 2** Comparison of determination of the predominant ramsdellite lattice parameters for differing sets of sharp *hkl* lines

| material | $a_T$ | $b_T$ | $c_T$ | set of lines |
|---|---|---|---|---|
| SBPA | 4.442±0.004 | 9.33±0.02 | 2.85±0.006 | $S_1$ [a] |
| SBPA | 4.435±0.004 | 9.25±0.04 | 2.85±0.006 | $S_{res}$ [b] |

[a] $S_1$ is the set of lines (021), (200), (121), (140), (221), (240), (002) and (061). [b] $S_{res}$ is the set of lines (021), (121), (221) and (002).

(because slight microtwinning affects the sharp lines[5]). Table 2 contains a comparison between the orthorhombic parameters obtained using the set of sharp lines used previously,[8] set $S_1$, and the set which was used in this work. As may be seen the restricted choice results in a slight shortening in the $b_T$ orthorhombic parameter and also a greater standard deviation on the same set of three measures. Nevertheless this procedure is still useful since it enables the variation in lattice parameters to be followed throughout the homogeneous insertion range. In order to represent and gain further insight into the measured expansions of the lattice parameters the following observations concerning the relationship between the most H-inserted and starting materials have been developed.

### Structural relationship between ramsdellite and groutite

Although γ-manganese dioxide contains de Wolff disorder, which implies a random succession of ramsdellite type layers and pyrolusite (rutile) type layers in the *b* direction, most of the manganese atoms in material SBPA are in ramsdellite type blocks. Since there are twice as many manganese atoms in a ramsdellite type layer compared to a pyrolusite type layer the fraction of which is equal to 41% for material SBPA (see Table 1) then the fraction of manganese in ramsdellite type layers is 74%. In the following, the predominant ramsdellite structure is discussed. A similar argument could also be applied to a structure where pyrolusite type layers predominate.

Consider Fig. 12 which displays a superposition of the ramsdellite ($MnO_2$) and groutite (MnOOH) structures in the *ab* plane. This diagram differs from previous comparisons[8] in that the unit cells are now centred at the corner of double octahedral chains. Such a procedure immediately brings out relationships between the structures which were not readily apparent in past comparisons. The two structures are now seen to exhibit different rotations about the common origin as well as having different octahedral sizes. The rotation is such that adjacent corner-connected chains of edge-shared double octahedra rotate in opposite directions. Thus if one chain of double octahedra exhibits clockwise rotation in transforming from ramsdellite to groutite then the four chains with which it is corner-connected are rotated anticlockwise by the same amount and so on throughout the crystal structure. This

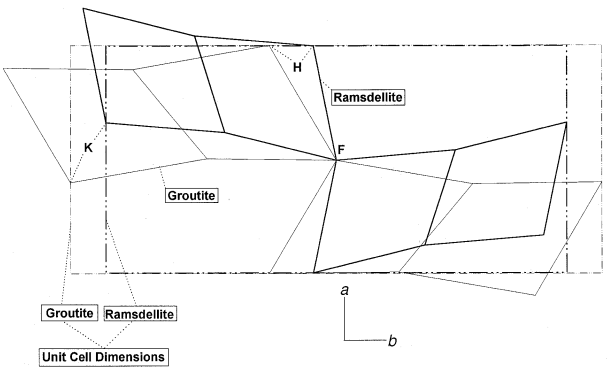


**Fig. 12** Comparison of groutite and ramsdellite: projection on *ab* plane

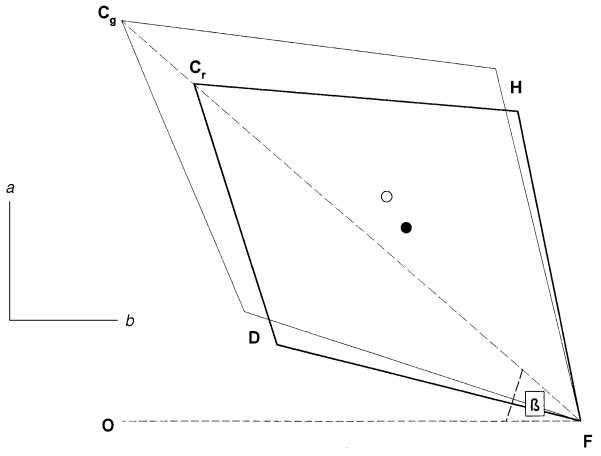


**Fig. 13** Comparison of groutite and ramsdellite octahedra projected on the *ab* plane

movement may be described as hinging about the lines of corner connection which run parallel to the *c* axis.

Superposition of the distorted octahedra of ramsdellite and groutite further reveals that the expansion is primarily in the direction of the line connecting apical oxygens normal to the *c* axis§ (*i.e.* in the direction $\mathbf{FC_r}$ or $\mathbf{FC_g}$, Fig. 13). This fact is predicted by crystal field theory[14,15] (CFT) for a $d^4$ electron configuration such as $Mn^{3+}$. Briefly, when a high-spin state obtains (*i.e.* a low crystal field) and the electron occupies the $d_{z^2}$ orbital then a distortion of the octahedra is favoured (lowering the energy of $d_{z^2}$ with respect to $d_{x^2-y^2}$) since this orbital is directed towards the apical oxygens. This effect is also known as Jahn–Teller distortion. Thus expansion of the octahedra primarily in the direction of the $d_{z^2}$ is expected for increasing H-insertion.

From the above argument no expansion is expected in the *c* direction, which is perpendicular to the *z* or apical oxygen direction. Thus the way in which the ramsdellite structure expands with H-insertion may be reduced to a two-dimensional problem with essentially two parameters, the expansion of the octahedra in the *z* direction and a measure of the hinging angle between adjacent double chains. The measure selected for the amount of hinging is the angle ($\beta$) that the apical oxygen line makes with the *b* axis (Fig. 13). As all that can be measured by powder XRD is the variation of *a*, *b* and *c* a structural map connecting the aforementioned parameters with the lattice parameters has been developed.

### Structural map of the H-insertion reaction

The projected octahedra in Fig. 13 are arranged such that the vectors $\mathbf{FC_r}$ and $\mathbf{FC_g}$ are aligned. $\mathbf{FC_g}$ in the fully H-inserted groutite structure is 18.67% larger than $\mathbf{FC_r}$ for ramsdellite. The effects of this expansion on the unit-cell parameters *a* and *b* are calculable using the coordinates of **H** and **K** based on **F** as the origin (Fig. 12). If the coordinates of **H** and **K** are known then so are the angles **HFO** (Fig. 13) and **KFO**. The calculation proceeded *via* a general formula capturing the effect of linear expansion in the **FC** direction. The other octahedral coordinates which underwent displacements were handled by interpolation using the same fractional expansion of the $\mathbf{FC_r}$ to $\mathbf{FC_g}$ transition. The procedure was shortened by recognizing that the point midway between $\mathbf{C_r}$ or $\mathbf{C_g}$ and **D** is an inversion centre, therefore once **C**, **D** and **H** are found, **K** can also be found. Letting $z = \mathbf{FC}$, the length of the apical line, the coordinates for the projected octahedra for 2% stepped intervals in *z* were calculated in the range 0–20%. At each incremental step the effects on the octahedral coordinates of rotation about point **F** of *z* (where angle $\mathbf{OFC} = \beta$) were also calculated so that the *a*, *b* lattice parameters for various degrees of hinging were obtained.

In this way a net was constructed enabling the percentage expansion *z* in the apical direction and rotation $\beta$ to be represented for given values of *a* and *b*. On this map are plotted the results for H-insertion into material SBPA (Fig. 14) for the lattice parameter variation derived from the lines $S_{res}$. As already discussed an apparent shortening of the *b* axis results from choosing the set of lines $S_{res}$ which explains why the starting materials ($s = 0$) lattice parameters show an apparent contraction with respect to ramsdellite. The shortened *a* axis, however, also occurs in the lattice parameters determined from line set $S_1$ as shown on Fig. 14. This value occurs close to the line of hinging without expansion. That is to say that material SBPA has lattice parameters consistent with a hinging of the ramsdellite structure since their *a* and *b* lattice parameters vary in exactly the way predicted by the two-parameter mode. It is tempting to explain the shortened *a* (and therefore the expanded *b* axis) as a result of the 41% pyrolusite type layers since SBPA possesses an *a* lattice dimension intermediate between those of pyrolusite ($a = 4.398$ Å[16]) and ramsdellite ($a = 4.533$ Å, JCPDS 39-375). On this basis the SBPA structure results from hinging the ramsdellite blocks so that its lattice parameter is reduced and matches that of pyrolusite layers which are hinged in the opposite direction so as to cause an expansion of the pyrolusite *a* lattice parameter.

H-insertion in the homogeneous region caused the structure to expand in the *z* or apical direction with little rotation. This means that the octahedra underwent continuous Jahn–Teller distortion in the homogeneous region since the dimensions of the octahedra for groutite and ramsdellite in the direction perpendicular to the apical direction (*i.e.* **DH**) are similar as can be seen from Fig. 13. Lattice expansion of the *a* and *b*

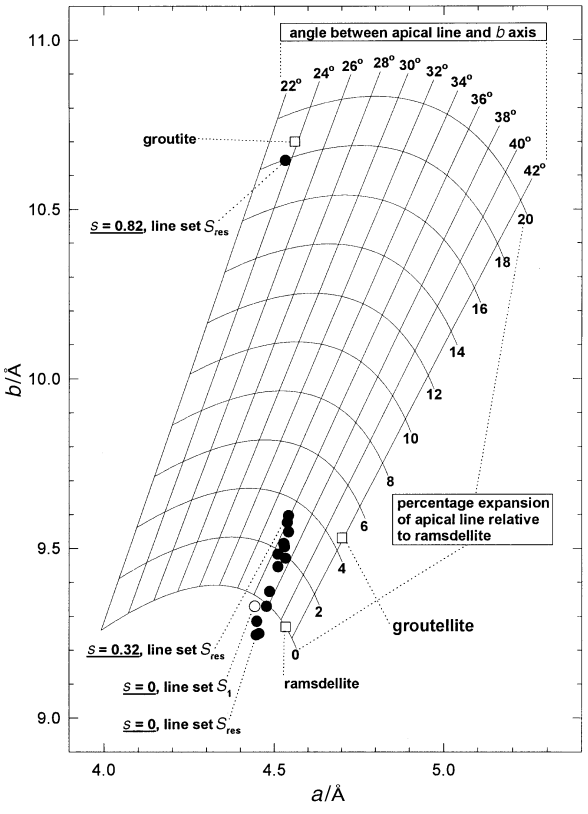


**Fig. 14** The effects of H-insertion on the percentage expansion in the apical direction *z* and rotation $\beta$ from the *a*, *b* lattice parameter variation for material SBPA

§ Although other apical lines exist this is the line meant throughout this work.

parameters was continuous up until the $a$ parameter matched that of the most H-inserted product whereupon heterogeneous insertion occurred. It seems significant that heterogeneous H-insertion only started when the apical expansion occurring in the homogeneous region had brought the $a$ lattice dimension to the same value as that of the fully H-inserted product. This coincidence of $a$ (and $c$) lattice parameters would allow H-insertion in the heterogeneous region to proceed in the $b$ direction by movement of an almost seamless boundary in an $ac$ plane between reactant ($s=0.34$) and product ($s=0.82$).

Fig. 14 shows that the lattice parameters of the most H-inserted product are close to those of groutite and are the result of an apical expansion of 18% relative to ramsdellite and hinging which changes $\beta$ from about 35° ($s=0.34$) to $<24°$ ($s=0.82$). As may be deduced from Fig. 12 this change in hinging angle alters the cross-section of the $[2\times1]$ tunnels from essentially rectangular in the reactant for the heterogeneous region ($s=0.34$) to essentially parallelograms for the product ($s=0.82$). The FTIR study provided evidence for OH bond formation in the product in contrast to its absence in the reactant. It is compelling to link the change in shape of the $[2\times1]$ tunnels with OH bond formation. In fact the change in shape brings the O(2) sites (oxygens pyramidically coordinated with three manganese atoms) closer to the O(1) sites thus allowing inserted H to bond with one type of oxygen and form a hydrogen bond with the other type as previously suggested for EMD.[3]

Previous reports of a large change in the Jahn–Teller distortion parameter[1,3,4] which was defined as the ratio of two sides of an octahedron $a''/a'$ where

$$a'=c, \quad a''=0.5[(b^2/4)+c^2]^{\frac{1}{2}} \tag{4}$$

may be questioned. Eqn. (4) gives $a''/a'=1$ when $b=2\sqrt{3}c$, the requirement for hcp oxygens (*i.e.* perfect octahedra). However, as may now be appreciated, $b$ or $a$ may change without distortion of the octahedra by rotation of the apical direction $z$. Thus the ratio $a''/a'$ calculated from eqn. (4) does not properly reflect distortion of an octahedron. Previous work by Giovanoli *et al.*,[4] also on a low microtwinned material, has also not considered the possibility that a heterogeneous reaction may obtain after a given level of insertion which on re-examination of their data seems likely.

Also shown on the structural map (Fig. 14) is the mineral believed to be groutellite[5] (JCPDS card 42-1316), an intermediate mineral always found in small quantities associated with ramsdellite[17] which is supposed to have the composition $MnOOH_{0.5}$. Its position with respect to ramsdellite indicates that it is properly described as an expanded form of ramsdellite since the changes in lattice parameters are very nearly explained by an expansion of the octahedra in the $z$ direction with less than a 2° change in $\beta$, which is fairly similar to the behaviour for insertion into SBPA.

It should be noted that the above analysis is valid only if the magnitude of the $c$ lattice parameter does not vary. Published data on ramsdellite, groutellite and groutite (JCPDS cards 39-375, 42-1316 and 24-713 respectively) indicate their $c$ dimensions are nearly equal (greatest difference 0.21%) as expected since the $z$ direction is perpendicular to $c$. Similarly the $c$ direction, as determined from the lines $S_{res}$, varied by 0.4% for material SBPA at $s=0.32$ and by 0.7% at $s=0.82$ relative to the starting material $s=0.00$.

## Conclusions

The conclusions from this work are as follows.

(1) Chemical H-insertion into a low microtwinned $\gamma$-manganese dioxide in the insertion range $0.00\leqslant s\leqslant0.34$ proceeded by homogeneous reaction consistent with the formation of a solid solution with mobile H.

(2) The structure expanded in accordance with each $Mn^{3+}$ occupied octahedron stretching in the apical direction, *i.e.* a continuously increasing Jahn–Teller distortion was observed.

(3) Insertion in the range $0.34\leqslant s\leqslant0.82$ proceeded by heterogenous two-phase reaction in which the most inserted compound contained inserted H located in OH bonds in contrast to the absence of such bonds in the reactant ($s=0.34$).

(4) The structure of the fully inserted compound was $\delta$-MnOOH, which contains occupied double chains of octahedra both expanded in the apical direction and hinged with respect to the starting material in a manner similar to that of the minerals groutite and ramsdellite.

(5) Evidence for a link between hinging of the structure and the location of H was discovered.

(6) The predominant lattice parameters of the starting material SBPA are consistent with a rotation of the apical line $z$ by 4° with respect to ramsdellite, due probably to the influence of de Wolff faults.

The authors wish to thank Dr. Ernst Preisler who kindly donated the SBP-EMD and Dr. Dom Swinkels for carrying out the FTIR measurements.

### References

1 J. P. Gabano, B. Morignat, E. Fialdes, B. Emery and J. F. Laurent, *Z. Phys. Chem.*, 1965, **46**, 359.
2 J. Fitzpatrick and F. L. Tye, *J. Appl. Electrochem.*, 1991, **21**, 130.
3 W. C. Maskell, J. E. A. Shaw and F. L. Tye, *Electrochim. Acta*, 1981, **26**, 1403.
4 R. Giovanoli, K. Bernhard and W. Feitknecht, *Helv. Chim. Acta*, 1969, **52**, 2333.
5 Y. Chabre and J. Pannetier, *Prog. Solid State Chem.*, 1995, **23**, 1.
6 F. L. Tye and S. W. Tye, *J. Appl. Electrochem.*, 1995, **25**, 425.
7 J. Fitzpatrick, L. A. H. MacLean, D. A. J. Swinkels and F. L. Tye, *J. Appl. Electrochem.*, 1997, **27**, 243.
8 L. A. H. MacLean and F. L. Tye, *J. Solid State Chem.*, 1996, **123**, 150.
9 E. Preisler, *J. Appl. Electrochem.*, 1989, **19**, 540.
10 P. Strobel, J-C. Joubert and M-J. Rodriguez, *J. Mater. Sci.*, 1986, **21**, 583.
11 K. J. Vetter and N. Yeager, *Electrochim. Acta*, 1966, **11**, 401.
12 P. M. de Wolff, *Acta Crystallogr.*, 1959, **12**, 341.
13 C. Chatfield, *Statistics for Technology*, Chapman and Hall, London, 3rd edn., 1985, p. 306.
14 *The Chemistry of the Transition Elements*, ed. A. Earnshaw and T. J. Harrington, Clarendon Press, Oxford, 1973, p. 24.
15 T. Ohzuku, J. Kato, K. Sawai and T. Hirai, *J. Electrochem. Soc.*, 1991, **138**, 2557.
16 W. H. Baur, *Acta Crystallogr., Sect. B*, 1976, **32**, 2200.
17 J. F. Post and R. D. Ross, *Eos* (*Madrid*), 1989, **70**, 352.

*Paper* 6/08232G; *Received* 6*th December*, 1996